changes in the maximal rate of Ca^{2+} pump activity (V_{max}) in any of our genotypes (table S2). Because DWORF is most abundant in the slow-twitch soleus muscle group, we also measured SERCA activity in soleus homogenates from WT and KO mice and used quadriceps muscles as a control, because DWORF is not expressed in this muscle group. Analysis of homogenates from the soleus muscle of *Dworf* KO mice revealed a decreased apparent affinity of SERCA for Ca^{2+} as compared with homogenates from WT muscles (Fig. 4B and table S3). These differences were not observed in quadriceps muscle (figs. S14B and table S4).

To determine whether DWORF directly activates SERCA or does so through displacement of its endogenous inhibitors, we cotransfected COS7 cells with SERCA2a and DWORF in the presence or absence of PLN, SLN, and MLN (*4*). We found that coexpression of DWORF alone with SERCA2a did not change the apparent affinity of SERCA for Ca^{2+}, but it relieved the inhibition by PLN in a dose-dependent manner (fig. S15). Threefold overexpression of DWORF was sufficient to return SERCA activity to baseline levels when coexpressed with PLN, SLN, or MLN (fig. S16). These results indicate that DWORF counteracts the effect of inhibitory peptides rather than directly stimulating SERCA pump activity, which is consistent with the lack of primary sequence similarity between DWORF and SERCA inhibitors (fig. S17).

Based on gain- and loss-of-function studies, our results demonstrate that DWORF enhances SR Ca^{2+} uptake and myocyte contractility through its displacement of the inhibitory peptides PLN, SLN, and MLN from SERCA (Fig. 4C). Because DWORF increases the activity of the SERCA pump, it represents an attractive means of enhancing cardiac contractility in settings of heart disease. Finally, our results underscore the likelihood that many transcripts currently annotated as noncoding RNAs encode peptides with important biological functions. These small peptides may evolve rapidly as singular functional domains that fine-tune the activities of larger preexisting molecular complexes, rather than having intrinsic biologic effects themselves. In this regard, small peptides may be uniquely suited to act as key factors in evolutionary adaptation and speciation.

REFERENCES AND NOTES

1. D. M. Bers, *Nature* **415**, 198–205 (2002).
2. D. H. MacLennan, M. Asahi, A. R. Tupling, *Ann. N. Y. Acad. Sci.* **986**, 472–480 (2003).
3. E. G. Kranias, R. J. Hajjar, *Circ. Res.* **110**, 1646–1660 (2012).
4. D. M. Anderson et al., *Cell* **160**, 595–606 (2015).
5. N. C. Bal et al., *Nat. Med.* **18**, 1575–1579 (2012).
6. E. G. Magny et al., *Science* **341**, 1116–1120 (2013).
7. G. W. Dorn 2nd, J. D. Molkentin, *Circulation* **109**, 150–158 (2004).
8. S. A. Slavoff et al., *Nat. Chem. Biol.* **9**, 59–64 (2013).
9. M. C. Frith et al., *PLOS Genet.* **2**, e52 (2006).
10. B. R. Nelson, D. M. Anderson, E. N. Olson, *Circ. Res.* **114**, 18–20 (2014).
11. M. F. Lin, I. Jungreis, M. Kellis, *Bioinformatics* **27**, i275–i282 (2011).
12. C. Xie et al., *Nucleic Acids Res.* **42** (D1), D98–D103 (2014).
13. E. L. Sonnhammer, G. von Heijne, A. Krogh, *Proc. Int. Conf. Intell. Syst. Mol. Biol.* **6**, 175–182 (1998).
14. A. Krogh, B. Larsson, G. von Heijne, E. L. Sonnhammer, *J. Mol. Biol.* **305**, 567–580 (2001).
15. M. Goujon et al., *Nucleic Acids Res.* **38** (Web Server), W695–W699 (2010).
16. A. N. Guido, G. E. Campos, H. S. Neto, M. J. Marques, E. Minatel, *Anat. Rec. (Hoboken)* **293**, 1722–1728 (2010).
17. S. Schiaffino, C. Reggiani, *Physiol. Rev.* **91**, 1447–1531 (2011).
18. J. D. Molkentin et al., *Cell* **93**, 215–228 (1998).
19. B. R. Nelson et al., *Proc. Natl. Acad. Sci. U.S.A.* **110**, 11881–11886 (2013).
20. M. Asahi, Y. Kimura, K. Kurzydlowski, M. Tada, D. H. MacLennan, *J. Biol. Chem.* **274**, 32855–32862 (1999).
21. A. R. Tupling et al., *Am. J. Physiol. Cell Physiol.* **301**, C841–C849 (2011).
22. B. A. Davis, A. Schwartz, F. J. Samaha, E. G. Kranias, *J. Biol. Chem.* **258**, 13587–13591 (1983).

METABOLISM

AMP-activated protein kinase mediates mitochondrial fission in response to energy stress

Erin Quan Toyama,[1]* Sébastien Herzig,[1]* Julien Courchet,[2] Tommy L. Lewis Jr.,[2] Oliver C. Losón,[3] Kristina Hellberg,[1] Nathan P. Young,[1] Hsiuchen Chen,[3] Franck Polleux,[2] David C. Chan,[3] Reuben J. Shaw[1]†

Mitochondria undergo fragmentation in response to electron transport chain (ETC) poisons and mitochondrial DNA–linked disease mutations, yet how these stimuli mechanistically connect to the mitochondrial fission and fusion machinery is poorly understood. We found that the energy-sensing adenosine monophosphate (AMP)–activated protein kinase (AMPK) is genetically required for cells to undergo rapid mitochondrial fragmentation after treatment with ETC inhibitors. Moreover, direct pharmacological activation of AMPK was sufficient to rapidly promote mitochondrial fragmentation even in the absence of mitochondrial stress. A screen for substrates of AMPK identified mitochondrial fission factor (MFF), a mitochondrial outer-membrane receptor for DRP1, the cytoplasmic guanosine triphosphatase that catalyzes mitochondrial fission. Nonphosphorylatable and phosphomimetic alleles of the AMPK sites in MFF revealed that it is a key effector of AMPK-mediated mitochondrial fission.

Metabolic stresses that inflict damage to mitochondria trigger mitochondrial fragmentation, leading to degradation of defective mitochondria (mitophagy) or apoptosis in cases of severe damage (*1*). This response enables the consolidation of the still-intact functional elements of mitochondria, while allowing for physical segregation of dysfunctional mitochondrial components into depolarized daughter organelles that are targeted for mitophagy (*2, 3*). Similarly, proper mitochondrial fission facilitates timely apoptosis (*4–7*). Mitochondrial fragmentation is also associated with mitochondrial dysfunction, such as in diseases associated with mitochondrial DNA (mtDNA) mutations (*8*). Conversely, mitochondrial fusion is thought to promote oxidative phosphorylation (*9*), to spare mitochondria from mitophagy (*10, 11*), and to allow biodistribution of fatty acids for fuel utilization under nutrient-limited conditions to maintain metabolite pools and efficient adenosine triphosphate (ATP) production (*12*).

A central metabolic sensor activated by a wide variety of mitochondrial insults is the adenosine

¹Molecular and Cell Biology Laboratory and Howard Hughes Medical Institute, Salk Institute for Biological Studies, La Jolla, CA 92037, USA. ²Department of Neuroscience, Zuckerman Mind Brain Behavior Institute and Kavli Institute for Brain Science, Columbia University, New York, NY 10032, USA. ³Division of Biology and Biological Engineering, California Institute of Technology, Pasadena, CA 91125, USA.
*These authors contributed equally to this work.
†Corresponding author. E-mail: shaw@salk.edu

monophosphate (AMP)–activated protein kinase (AMPK) (13). Under conditions when intracellular ATP concentrations decrease, increased intracellular AMP directly binds to the γ regulatory subunit of AMPK, facilitating AMPK activation by the upstream protein kinase LKB1. Upon activation, AMPK restores intracellular energy levels through direct phosphorylation of multiple downstream substrates that inhibit ATP-consuming biosynthetic pathways and stimulate catabolic ATP-regenerating processes. Because mitochondria supply the majority of cellular ATP, the maintenance of mitochondrial function is critical to maintaining overall energetic homeostasis (14), but the question of whether AMPK plays direct roles in different aspects of mitochondrial biology has not been well examined. AMPK has previously been tied to mitochondrial integrity through its direct phosphorylation and activation of the highly conserved autophagy kinase ULK1 (Atg1 in yeast) (15, 16), which promotes mitophagy. In comparison, although mitochondrial fission and fusion rates are known to respond to changes in cellular metabolism, the molecular details of how changes in cellular bioenergetics and nutrients couple to the fission and fusion machinery remain poorly understood (17). For example, cells treated with mitochondrial inhibitors or bearing mtDNA-linked mutations undergo mitochondrial fragmentation, but much of the biochemical underpinning for these effects remains obscure. Inhibition of mitochondrial fusion due to aberrant processing of Optic atrophy 1 (OPA1, an inner mitochondrial membrane fusion GTPase) is a proposed mechanism (17–21), but it is thought to require a loss of mitochondrial membrane potential, which does not occur with many fragmentation-inducing stimuli.

We examined whether AMPK plays a part in the dynamic response of mitochondria to lowered ATP concentrations. To this end, we treated human U2OS osteosarcoma cells with the electron transport chain (ETC) complex I inhibitor rotenone or complex III inhibitor antimycin A for 1 hour and assessed their mitochondrial morphology. Confocal microscopy of endogenous TOM20 staining revealed extensive fragmentation of mitochondria caused by both inhibitors (Fig. 1A, top row). Time-lapse microscopy with MitoTracker dye to visualize live fusion and fission events revealed extensive mitochondrial fragmentation within 30 min after the addition of rotenone (Fig. 1B and movie S1). Treatment with either rotenone or antimycin A led to the rapid activation of AMPK and phosphorylation of its well-established downstream substrates acetyl coenzyme A carboxylase (ACC), Raptor, and ULK1 within 15 min (Fig. 1C).

We next used CRISPR/Cas9 to genetically disrupt the two catalytic subunits of AMPK (AMPKα1 and AMPKα2) in U2OS cells (AMPK double knockout, DKO) (fig. S1A). We demonstrated that both AMPK catalytic subunits must be genetically removed in U2OS cells to fully abolish AMPK signaling in this cell type (Fig. 1C and fig. S1B), similar to what is observed in other cell types (22). In AMPK DKO U2OS cells, the effect of ro-

tenone or antimycin A on mitochondrial fragmentation was significantly attenuated (Fig. 1, A and D), as visualized by TOM20 staining at fixed time points (Fig. 1A) and by time-lapse microscopy (Fig. 1B and movie S2), despite comparable effects on oxygen consumption rates (fig. S1C). Lentivirus was used to stably reconstitute a wild-type AMPKα1 or AMPKα2 cDNA into the AMPK DKO U2OS cells to confirm that the loss of mitochondrial fragmentation was not an artifact of the chosen AMPK DKO clone. In cells treated with rotenone and antimycin A, either reconstituted AMPKα1 or AMPKα2 was sufficient to restore mitochondrial fragmentation and phosphorylation of downstream substrates, suggesting that either of the α subunits is capable of mediating these responses in U2OS cells (Fig. 1, A and D, and fig. S1D).

Some stimuli that acutely trigger mitochondrial fragmentation lead to proteolytic cleavage and inactivation of the OPA1 GTPase that mediates inner mitochondrial membrane fusion (17–21). We therefore compared the induction of AMPK activation with the induction of OPA1 proteolytic cleavage. Although the ETC uncoupler CCCP (carbonyl cyanide m-chlorophenyl hydrazone) promoted OPA1 processing, this effect was absent in cells treated with rotenone or antimycin A (fig. S1E), supporting reports that a loss of mitochondrial membrane potential is required for OPA1 cleavage (17–20). Immunoblotting of wild-type and AMPK DKO cells after CCCP treatment revealed that OPA1 cleavage was independent of AMPK status, reinforcing that these are two independent biochemical events. AMPK is activated by a loss of ATP due to ETC inhibition, whereas OPA1 cleavage is induced only after the more extensive mitochondrial damage that accompanies a loss of mitochondrial membrane potential.

We next examined whether direct pharmacological activation of AMPK in the absence of mitochondrial inhibitor treatment would be sufficient to induce mitochondrial fission. The small molecule A769662 and related compounds (MT63-78 and 991) were isolated from high throughput screens for AMPK activators (23–25). All of the A769662-related compounds are thought to bind in a cleft between the AMPK α and β subunits, in contrast to AMP-mimetic compounds such as AICAR (5-aminoimidazole-4-carboxamide ribonucleotide), which bind to nucleotide binding pockets in AMPKγ subunits to trigger activation of AMPK kinase complexes (26). Treatment of U2OS cells with A769662 for 1 hour resulted in mitochondrial fragmentation equivalent to that which occurred after rotenone or antimycin A treatment (compare Fig. 2, A to C, with Fig. 1, A, B, and D). This effect was almost fully ablated in the AMPK DKO U2OS cells (Fig. 2, A and B, and fig. S2A). Similarly, the cell-permeable AMP-mimetic AICAR increased the percentage of cells with short mitochondria, an effect ablated in the AMPK DKO U2OS cells (Fig. 2, A and B). The effects of these two mechanistically distinct direct AMPK activators on mitochondrial fragmentation were restored in the AMPK DKO U2OS

cells that were stably reconstituted with either wild-type AMPKα1 or AMPKα2 cDNAs (Fig. 2, A and B), which also restored full downstream AMPK signaling (fig. S2B).

We also assessed AMPK induction of mitochondrial fragmentation in SV40-immortalized murine embryonic fibroblasts (MEFs) bearing floxed alleles of AMPKα1 (Prkaa1) and AMPKα2 (Prkaa2) that we derived de novo from embryonic day–13 mouse embryos to ensure equivalent starting mitochondrial populations. These cells were transduced with adenoviruses bearing either the Cre recombinase or the FlpO recombinase to obtain parallel treated cultures in which both AMPKα1 and AMPKα2 were deleted or that were exposed to a nontargeting control recombinase, respectively. Immunoblotting confirmed efficient deletion of AMPKα1 and AMPKα2 and a loss of downstream signaling only in the Cre-treated cells (fig. S2C). Mitochondrial networks in MEFs are shorter and less tubulated under basal conditions compared with those in U2OS cells, but treatment with rotenone further induced fragmentation of mitochondria in wild-type MEFs, which was largely ablated in the AMPK DKO MEFs (Fig. 2, D and E). Direct activation of AMPK with MT63-78 (a more potent A769662 derivative) (25) induced acute mitochondrial fragmentation in MEFs to an extent comparable to that with rotenone treatment, which was also attenuated in the AMPK DKO MEFs (Fig. 2, D and E). The observation that mechanistically distinct AMPK activators can consistently induce fragmentation to the same extent as ETC inhibitors, across cell types with morphometrically distinct mitochondrial networks, suggests that AMPK may directly regulate some component(s) of the mitochondrial fission and fusion machinery to mediate these events.

Previously, our laboratory has used proteomic and bioinformatics approaches to identify AMPK substrates (15, 27–29). In one screen for AMPK substrates, we identified a protein named C2orf33, which subsequently was renamed mitochondrial fission factor (MFF). MFF is a mitochondrial outer-membrane protein that was discovered in an RNA interference screen aimed at identifying factors required for mitochondrial fission (30). Mitochondrial fission involves the recruitment of the GTPase dynamin-related protein 1 (DRP1) from the cytosol to the mitochondrial surface to catalyze the fission reaction. Genetic analysis has demonstrated that MFF is the dominant receptor for DRP1 in most mammalian cell types examined to date (31–33). MFF contains two predicted candidate AMPK phosphorylation sites, Ser[155] and Ser[172] in human MFF, which lie between the DRP1-interacting region at the amino terminus and the mitochondrial targeting transmembrane domain at the carboxyl terminus (Fig. 3A and fig. S3A). MFF was directly phosphorylated by recombinant AMPK, and, although mutation of Ser[172] attenuated most of the in vitro phosphorylation, it was only fully ablated when Ser[155] was also mutated (Fig. 3B). We used phosphomotif antibodies directed against the AMPK optimal substrate motif (27) or the optimal 14-3-3 binding

motif to determine whether they recognize MFF phosphorylated at Ser[155] or Ser[172] in vivo. FLAG-tagged variants of MFF cDNAs were stably introduced into wild-type MEFs, and treatment of the cells with AICAR increased MFF phos-phorylation (Fig. 3C). A nonphosphorylatable Ser172Ala mutation abolished interaction with the antibody to the 14-3-3 binding motif, whereas a nonphosphorylatable Ser155Ala mutation abolished the interaction with the antibody to the AMPK substrate motif, and mutation of either site alone did not affect the AICAR-induced phosphorylation of the other site (Fig. 3C). Phosphorylation of either site was largely ablated in the AMPK DKO MEFs (Fig. 3D).
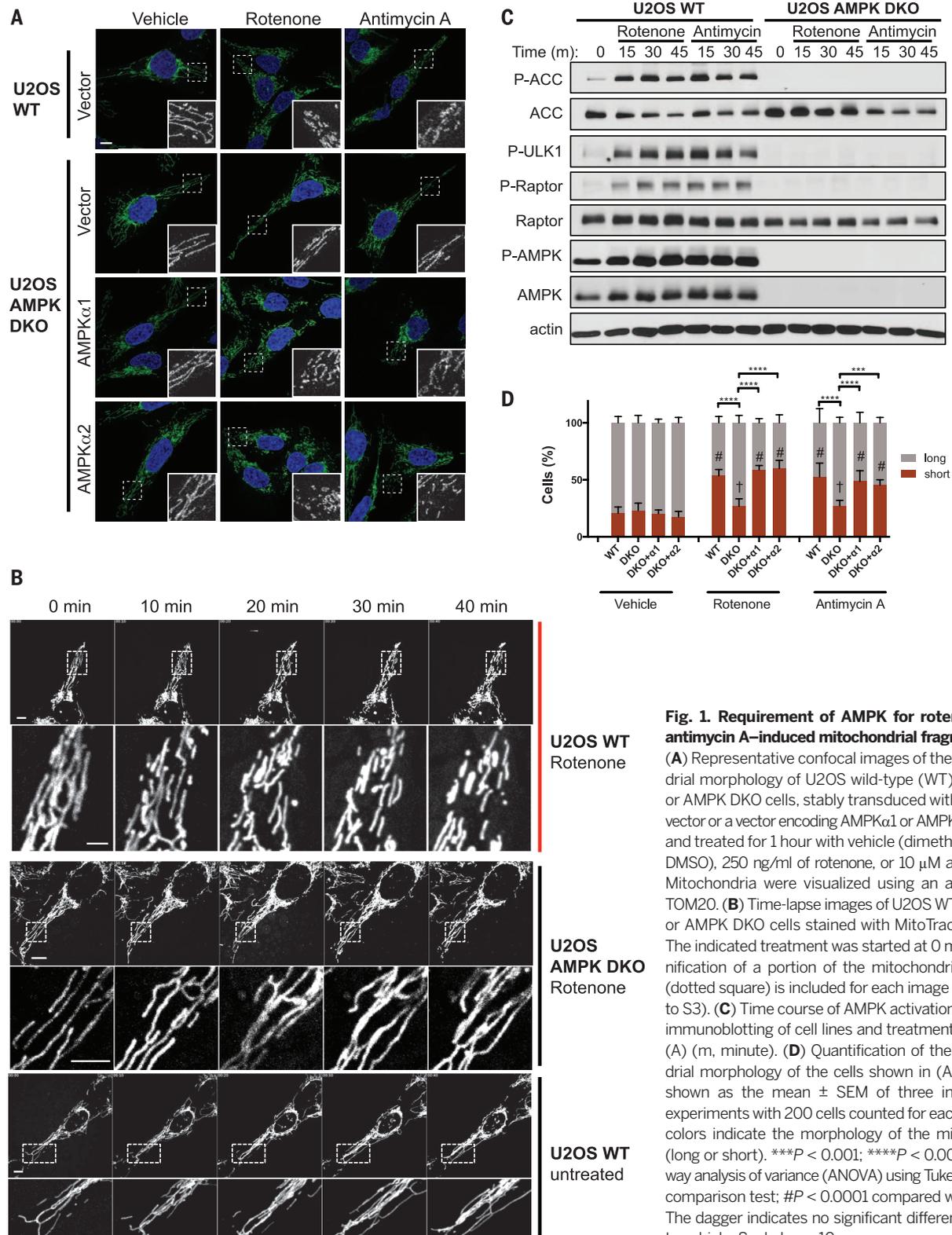

Fig. 1. Requirement of AMPK for rotenone- and antimycin A–induced mitochondrial fragmentation. (**A**) Representative confocal images of the mitochondrial morphology of U2OS wild-type (WT) (parental) or AMPK DKO cells, stably transduced with an empty vector or a vector encoding AMPKα1 or AMPKα2 cDNAs, and treated for 1 hour with vehicle (dimethyl sulfoxide, DMSO), 250 ng/ml of rotenone, or 10 μM antimycin A. Mitochondria were visualized using an antibody to TOM20. (**B**) Time-lapse images of U2OS WT (parental) or AMPK DKO cells stained with MitoTracker Green. The indicated treatment was started at 0 min. A magnification of a portion of the mitochondrial network (dotted square) is included for each image (movies S1 to S3). (**C**) Time course of AMPK activation by protein immunoblotting of cell lines and treatments shown in (A) (m, minute). (**D**) Quantification of the mitochondrial morphology of the cells shown in (A). Data are shown as the mean ± SEM of three independent experiments with 200 cells counted for each replicate; colors indicate the morphology of the mitochondria (long or short). ***$P < 0.001$; ****$P < 0.0001$ by two-way analysis of variance (ANOVA) using Tukey's multiple comparison test; #$P < 0.0001$ compared with vehicle. The dagger indicates no significant difference relative to vehicle. Scale bars, 10 μm.
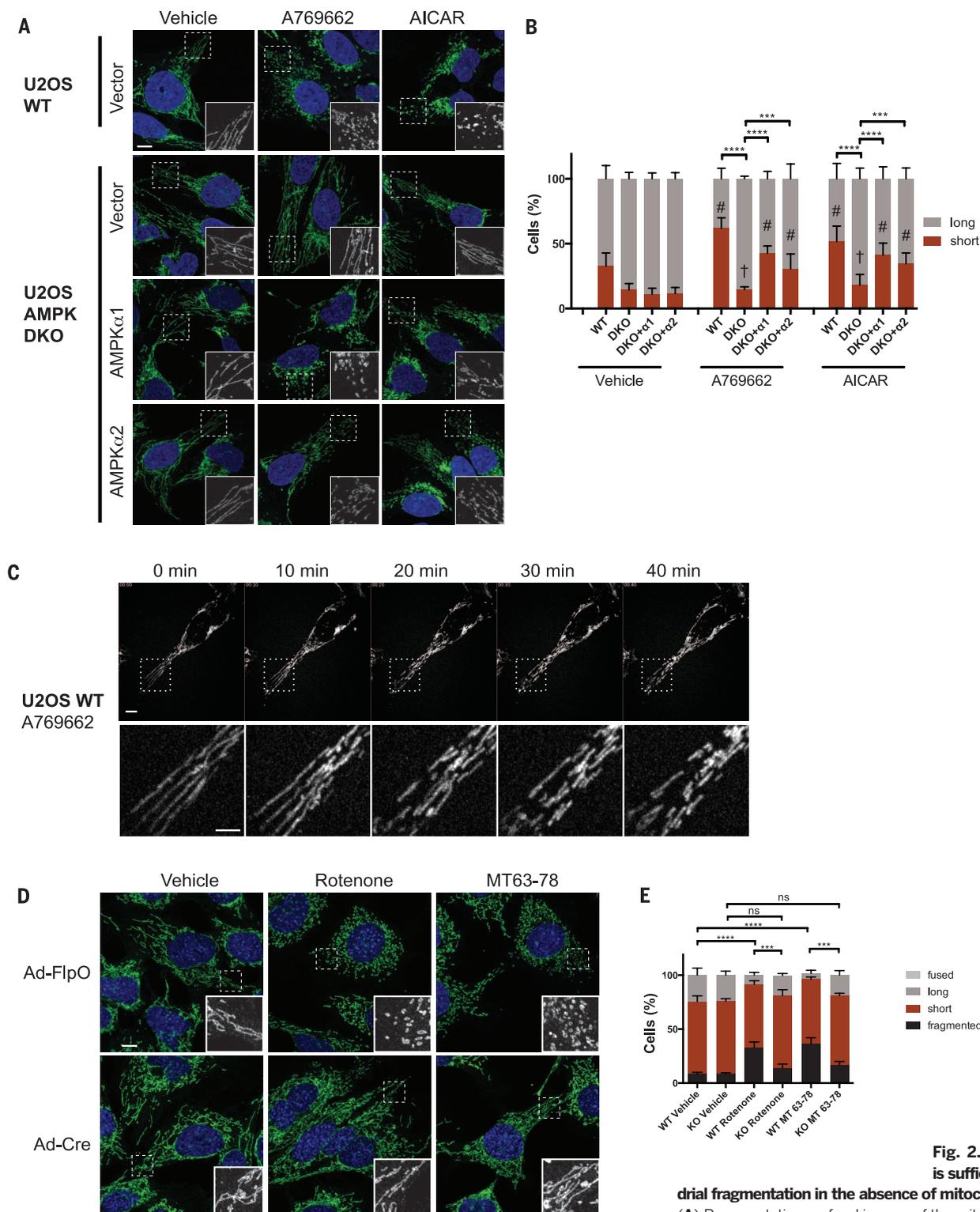
Fig. 2. AMPK activation is sufficient for mitochondrial fragmentation in the absence of mitochondrial inhibitors. (**A**) Representative confocal images of the mitochondrial morphology of WT (parental) or AMPK DKO U2OS cells, stably transduced with an empty vector or a vector encoding human AMPKα1 or AMPKα2 cDNAs, and treated for 1 hour with vehicle (DMSO), 300 μM A769662, or 2 mM AICAR. Mitochondria were visualized using an antibody to TOM20. (**B**) Quantification of the mitochondrial morphology of cells shown in (A). (**C**) Time-lapse images of WT (parental) U2OS cells stained with MitoTracker Green and treated with 300 μM A769662 at 0 min. A magnification of a portion of the mitochondrial network (dotted square) is included for each image (bottom panel; movie S4). (**D**) Representative confocal images of the mitochondrial morphology of AMPKα1$^{fl/fl}$α2$^{fl/fl}$ (fl, floxed) MEFs transduced with FlpO (control)– or Cre-encoding adenoviruses (Ad) and treated for 1 hour with vehicle (DMSO), 100 ng/ml of rotenone, or 50 μM MT63-78. Mitochondria were visualized using an antibody to TOM20. (**E**) Quantification of the mitochondrial morphology of cells shown in (D). Data in (B) and (E) are shown as the mean ± SEM of three independent experiments with 200 cells counted for each replicate and statistically analyzed as in Fig. 1 (ns, not significant). Scale bars, 10 μm.

To examine endogenous MFF phosphorylation, we developed a phosphospecific antibody to phospho-Ser[172] (P-Ser[172]), which we validated for phosphospecificity and induction in cells either expressing an activated allele of AMPK or treated with metabolic stress (fig. S3, B and C). Multiple alternatively splice isoforms of MFF have been documented, and one of the differentially spliced exon boundaries in MFF occurs just after Ser[172] (fig. S3D) (34). However, direct exam-

ination of transiently expressed cDNAs of MFF splice isoforms revealed that the antibody to P-Ser[172] recognized the cognate site in an AMPK-dependent manner in three of four isoforms tested (fig. S3D). To next ascertain whether the antibody to P-Ser[172] recognized endogenous MFF, we used MEFs genetically lacking MFF (fig. S4A). AICAR treatment induced reactivity of endogenous MFF with the antibody to MFF P-Ser[172] in wild-type but not in the *Mff*-null MEFs (fig. S4B). Next, we immuno-

blotted parallel lysates from AMPK wild-type and genetically matched DKO MEFs treated with rotenone or MT63-78, in which AMPK was critical for mitochondrial shortening (Fig. 2, D and E). This revealed that endogenous MFF P-Ser[172] was increased in wild-type but not AMPK DKO MEFs after receiving these stimuli (fig. S4C). In time-course experiments, MFF P-Ser[172] was fully induced within 15 min of treatment of wild-type MEFs with rotenone, paralleling the timing of

Fig. 3. MFF is a conserved substrate of AMPK. (**A**) ClustalW alignment of two conserved sites on MFF that match the AMPK optimal substrate motif. Ser[172] (S172) matches the well-defined AMPK motif found in most substrates (27, 39), and Ser[155] (S155) contains additional selections including +4N that also have been previously described (39). (**B**) Incorporation of γ-^{32}P-ATP into MFF in vitro. Human embryonic kidney–293 T cells transfected with empty vector (mock), WT MFF, or the indicated MFF mutants were lysed, and the FLAG immunoprecipitates were combined with recombinant (recomb) active AMPK where indicated and γ-^{32}P-ATP in an in vitro kinase reaction. Proteins were resolved on a SDS–polyacrylamide gel electrophoresis gel, and parallel nonradioactive kinase assays were immunoblotted as indicated. (**C**) Phosphorylation of MFF mutants. WT MEFs stably expressing a control vector (mock), WT MFF, or the indicated MFF mutants were treated with vehicle or 2 mM AICAR for 1 hour. FLAG immunoprecipitates and lysates were immunoblotted with the indicated antibodies and phosphomotif antibodies that recognize phosphorylated Ser[172] or Ser[155]. (**D**) Phosphorylation in WT ([+/+]) or AMPK DKO ([−/−]) MEFs stably expressing a control vector (mock) or WT MFF. Cells were treated with vehicle or 2 mM AICAR for 1 hour and processed as in (C). (**E**) Protein immunoblot showing the time course of AMPK activation in WT and AMPK DKO MEFs, as generated in Fig. 2D, after treatment with 250 ng/ml of rotenone for the indicated times. Phosphorylation of endogenous MFF was detected by the antibody to MFF P-Ser[172]. (**F**) Protein immunoblot of primary hepatocytes prepared from WT or AMPK DKO livers and treated with increasing concentrations of metformin (0, 0.5, 1.0, and 2.0 mM), showing phosphorylation of endogenous MFF as detected by the antibody to MFF P-Ser[172].
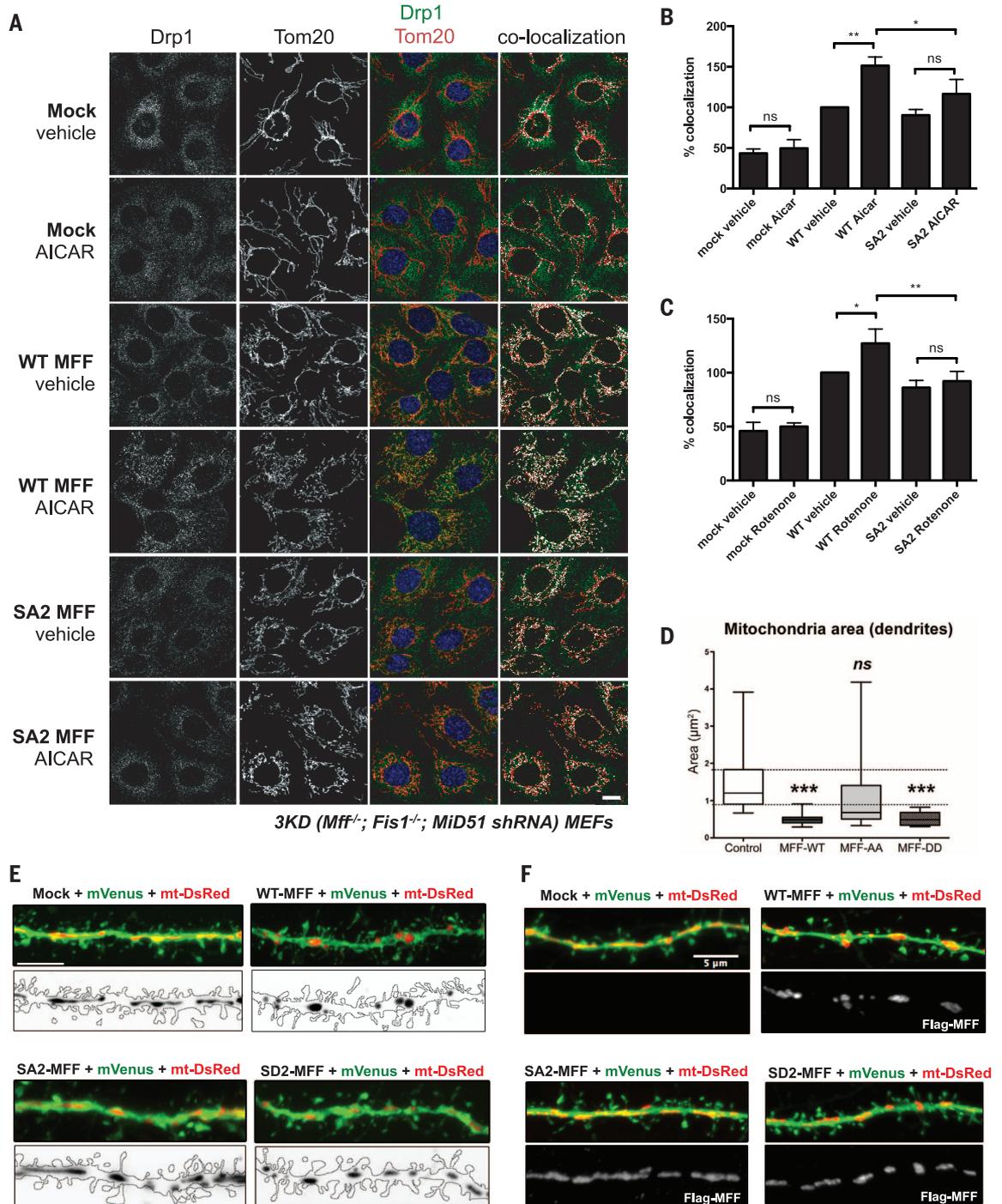
mitochondrial fragmentation and phosphorylation of other AMPK substrates (Fig. 3E). Mitochondrial morphology is altered in hepatocytes upon genetic deletion of AMPK (15); we therefore also examined MFF in this cell type. AICAR treatment of primary hepatocytes induced phosphorylation of endogenous MFF Ser^{172} and other AMPK substrates (fig. S4D). Another mitochondrial inhibitor that activates AMPK is metformin, the most-widely prescribed type 2 diabetes drug in the United States and worldwide (2). Metformin treatment of hepatocytes resulted in

Fig. 4. MFF Ser^{155} and Ser^{172} are required for recruitment of DRP1 to mitochondria after AMPK activation. (**A**) Representative images of 3KD MEFs stably transduced with a control vector (mock), WT MFF, or the SA2 MFF mutant, treated for 1 hour with vehicle (DMSO) or 2 mM AICAR and fixed and visualized with antibodies to endogenous TOM20 and DRP1. The merge of both channels as well as the result of the colocalization highlighter plugin (ImageJ) are shown. Scale bar, 10 μm. (**B**) Quantification of mitochondrial DRP1 in samples shown in (A) (details are included in the supplementary materials). Data are shown as the mean ± SEM of four independent experiments, each with at least five images representing >40 cells per condition. *$P < 0.05$; **$P < 0.01$ by one-way ANOVA. (**C**) Quantification of mitochondrial DRP1 after treatment with 250 ng/ml of rotenone for 1 hour, as in panels (A) and (B). (**D**) Quantification of the in vivo dendritic mitochondrial area upon overexpression of mVenus, mt-DsRED, and the indicated construct (AA, SA2; DD, SD2). Data are shown as 0 to 100% whisker box plots with the 25th, 50th, and 75th percentiles as the lower, middle, and upper boundaries of the box, respectively. Data were analyzed using a nonparametric Kruskal-Wallis ANOVA with Dunn's multiple comparisons ($n_{Control}$ = 19 neurons, n_{MFF-WT} = 19 neurons, n_{MFF-AA} = 27 neurons, and n_{MFF-DD} = 26 neurons from four distinct animals per genotype). ***$P < 0.001$. (**E**) Maximum projection images of layer 2/3 postnatal day–30 apical dendrite branches, demonstrating mitochondrial morphology upon expression of the labeled constructs via in utero electroporation at embryonic day 15.5. The upper panel in each section is the merge of mVenus and mt-DsRED; the lower panel shows the outline of the cell and mt-DsRED. (**F**) Maximum projection images of 21-day in vitro apical dendrite collaterals from cortical neurons electroporated with the indicated constructs via ex utero electroporation at embryonic day 15.5. The upper panel in each section is the merge of mVenus and mt-DsRED; the lower panel shows MFF expression via staining by the antibody to FLAG. Scale bars, 5 μm.

phosphorylation of endogenous MFF Ser[172] in a dose- and time-dependent manner, paralleling AMPK phosphorylation of Raptor and ULK1—effects which were abolished in AMPK DKO hepatocytes (Fig. 3F).

To test the effects of AMPK phosphorylation on MFF function, we first used MEFs that we have previously reported as lacking most functional DRP1 receptors [$Mff^{-/-}$, $Fis1^{-/-}$, and $Mid51$ short hairpin–mediated RNA interference (shRNA), referred to as 3KD MEFs] (fig. S5A) (31). Mitochondrial shortening that was induced by AICAR in wild-type cells was abolished in the 3KD cells (fig. S5B). Reconstitution of the 3KD cells with wild-type MFF cDNA demonstrated that MFF expression alone was sufficient to restore mitochondrial fragmentation in response to AICAR (fig. S5C). Subsequent analysis of MEFs that were genetically disrupted only for MFF ($Mff^{-/-}$) revealed they were also completely defective for AICAR-induced fragmentation (fig. S5D).

As the major receptor for DRP1, MFF is required for steady-state localization of DRP1 to the mitochondria (31, 33). Reconstitution of the 3KD MEFs with a wild-type MFF cDNA revealed a much greater colocalization of endogenous DRP1 to the mitochondria when MFF expression was restored, as compared with the control vector (Fig. 4, A and B). Treatment of cells with AICAR further increased colocalization of endogenous DRP1 with TOM20 in 3KD MEFs reconstituted with wild-type MFF, but this treatment failed to do so in the luciferase control 3KD MEFs (Fig. 4, A and B). This increase in DRP1 and TOM20 colocalization was attenuated in the cells stably expressing nonphosphorylatable Ser155Ala-Ser172Ala (SA2) mutant MFF, though amounts of MFF and DRP1 were comparable across these stable cell lines (fig. S5E). Similar effects on DRP1 and TOM20 colocalization were observed in response to rotenone treatment in cells bearing wild-type versus SA2 MFF (Fig. 4C and fig. S5F). These data indicate that basal DRP1 localization to mitochondria is largely normal in the SA2 cells but that AICAR and rotenone induce acute recruitment of DRP1 to the mitochondria, and this effect is abolished when AMPK cannot phosphorylate Ser[155] and Ser[172] in MFF. To model the effects of AMPK phosphorylation, we created phosphomimetic Ser155Asp-Ser172Asp (SD2) and Ser155Glu-Ser172Glu (SE2) mutants. Despite being expressed at equal levels to wild-type MFF protein (fig. S6A), both the SD2 and SE2 MFF mutants displayed gain-of-function activity when introduced into 3KD or $Mff^{-/-}$ MEFs, resulting in shortened mitochondria even in the absence of stimuli, comparable to those induced by AICAR in cells expressing wild-type MFF (fig. S6, B to E). Moreover, neither AICAR nor MT63-78 treatment further shortened the mitochondria in SD2- and SE2-expressing cells (fig. S6, C to E). Fragmented mitochondria are correlated with increased production of reactive oxygen species (35). Consistent with this, among all the 3KD cell lines, SD2- and SE2-MFF expressing cells exhibited the greatest accumulation of reactive oxygen species after rotenone treatment (fig. S6F).

To examine the function of the AMPK-dependent phosphorylation of MFF in vivo, in a cell type in which the AMPK pathway plays critical roles and in which mitochondrial homeostasis is paramount (36, 37), we expressed wild-type, SA2, or SD2 MFF cDNAs in layer 2/3 cortical pyramidal neurons using in utero cortical electroporation (36). Co-electroporation of cDNAs encoding myristoylated (m)Venus and mt-DsRed enabled quantitative imaging of mitochondrial morphology in dendritic segments of single neurons 3 weeks after birth (fig. S7, A and B). In control neurons, mitochondria morphology in the dendrites of pyramidal neurons is elongated (Fig. 4D). In contrast, enforced equivalent expression of wild-type or SD2 but not SA2 MFF resulted in fragmented mitochondria in the dendrites (Fig. 4, D and E). All three forms of MFF (wild-type, SA2, and SD2) were targeted to mitochondria and expressed at similar levels (Fig. 4F and fig. S7C). These results indicate that MFF is sufficient to induce fragmentation of neuronal mitochondria in vivo and that this effect requires phosphorylation of Ser[155/172].

AMPK is rapidly activated by mitochondrial stress and acutely triggers mitochondrial fission, at least in part via phosphorylation of MFF. This rapid AMPK-dependent induction of mitochondrial fission may serve as one way for the cell to prepare to initiate mitophagy of those mitochondrial fragments that have extensive damage (38). Though AMPK is a highly conserved sensor of mitochondrial damage across eukaryotes, MFF is one of the first AMPK substrates to have been discovered to directly control mitochondrial biology. AMPK is also known to induce mitochondrial biogenesis in various tissues (13), and AMPK directly phosphorylates and activates the first component of the autophagy cascade, the kinase ULK1 (15). Thus, AMPK emerges as a master regulator of mitochondrial homeostasis, coupling fission to mitophagy and, after prolonged energy stress, signaling the nucleus to initiate biogenesis of new mitochondria to replace the damaged ones.

REFERENCES AND NOTES

1. P. Mishra, D. C. Chan, Nat. Rev. Mol. Cell Biol. 15, 634–646 (2014).
2. G. Benard et al., J. Cell Sci. 120, 838–848 (2007).
3. G. Twig et al., EMBO J. 27, 433–446 (2008).
4. S. Montessuit et al., Cell 142, 889–901 (2010).
5. M. Karbowski et al., J. Cell Biol. 159, 931–938 (2002).
6. R. J. Youle, M. Karbowski, Nat. Rev. Mol. Cell Biol. 6, 657–663 (2005).
7. D. R. Green, L. Galluzzi, G. Kroemer, Science 345, 1250256 (2014).
8. J. Q. Kwong, M. S. Henning, A. A. Starkov, G. Manfredi, J. Cell Biol. 179, 1163–1177 (2007).
9. M. Liesa, O. S. Shirihai, Cell Metab. 17, 491–506 (2013).
10. L. C. Gomes, G. Di Benedetto, L. Scorrano, Nat. Cell Biol. 13, 589–598 (2011).
11. A. S. Rambold, B. Kostelecky, N. Elia, J. Lippincott-Schwartz, Proc. Natl. Acad. Sci. U.S.A. 108, 10190–10195 (2011).
12. A. S. Rambold, S. Cohen, J. Lippincott-Schwartz, Dev. Cell 32, 678–692 (2015).
13. B. B. Kahn, T. Alquier, D. Carling, D. G. Hardie, Cell Metab. 1, 15–25 (2005).
14. M. M. Mihaylova, R. J. Shaw, Nat. Cell Biol. 13, 1016–1023 (2011).
15. D. F. Egan et al., Science 331, 456–461 (2011).
16. J. Kim, M. Kundu, B. Viollet, K. L. Guan, Nat. Cell Biol. 13, 132–141 (2011).
17. P. Mishra, V. Carelli, G. Manfredi, D. C. Chan, Cell Metab. 19, 630–641 (2014).
18. S. Ehses et al., J. Cell Biol. 187, 1023–1036 (2009).
19. N. Ishihara, Y. Fujita, T. Oka, K. Mihara, EMBO J. 25, 2966–2977 (2006).
20. B. Head, L. Griparic, M. Amiri, S. Gandre-Babbe, A. M. van der Bliek, J. Cell Biol. 187, 959–966 (2009).
21. S. Duvezin-Caubet et al., J. Biol. Chem. 281, 37972–37979 (2006).
22. K. R. Laderoute et al., Mol. Cell. Biol. 26, 5336–5347 (2006).
23. B. Cool et al., Cell Metab. 3, 403–416 (2006).
24. B. Xiao et al., Nat. Commun. 4, 3017 (2013).
25. G. Zadra et al., EMBO Mol. Med. 6, 519–538 (2014).
26. M. F. Calabrese et al., Structure 22, 1161–1172 (2014).
27. D. M. Gwinn et al., Mol. Cell 30, 214–226 (2008).
28. M. M. Mihaylova et al., Cell 145, 607–621 (2011).
29. Y. Li et al., Cell Metab. 13, 376–388 (2011).
30. S. Gandre-Babbe, A. M. van der Bliek, Mol. Biol. Cell 19, 2402–2412 (2008).
31. O. C. Losón, Z. Song, H. Chen, D. C. Chan, Mol. Biol. Cell 24, 659–667 (2013).
32. Q. Shen et al., Mol. Biol. Cell 25, 145–159 (2014).
33. H. Otera et al., J. Cell Biol. 191, 1141–1158 (2010).
34. S. Ducommun et al., Cell. Signal. 27, 978–988 (2015).
35. X. Qi, N. Qvit, Y. C. Su, D. Mochly-Rosen, J. Cell Sci. 126, 789–802 (2013).
36. J. Courchet et al., Cell 153, 1510–1525 (2013).
37. G. Mairet-Coello et al., Neuron 78, 94–108 (2013).
38. R. J. Youle, A. M. van der Bliek, Science 337, 1062–1065 (2012).
39. J. W. Scott, D. G. Norman, S. A. Hawley, L. Kontogiannis, D. G. Hardie, J. Mol. Biol. 317, 309–323 (2002).

SUPPLEMENTARY MATERIALS

www.sciencemag.org/content/351/6270/275/suppl/DC1
Materials and Methods
Supplementary Text
Figs. S1 to S7
Reference (40)
Movies S1 to S5